A critical comparison of high-speed VCSEL characterisation techniques

Christopher J. O'Brien, Marian L. Majewski, *Senior Member, IEEE,* and Aleksandar D. Rakic, *Member, IEEE*

Abstract

This paper critically compares, for the first time, common microwave and optical procedures used for the high-speed characterisation of vertical-cavity, surface-emitting lasers (VCSELs). The intrinsic small-signal modulation characteristics of a VCSEL are measured, and the related rate equation parameters are extracted. Observed trends show excellent agreement with theory. The modulation characteristics of the VCSEL are determined by examining three different responses: relative intensity noise, S21 response, and high-resolution optical spectra. The various experimental techniques yielded consistent results. The relative strengths and weaknesses of each measurement are investigated below.

Index Terms

VCSEL, relative intensity noise (RIN), relaxation resonance frequency.

The authors are with the School of Information Technology and Electrical Engineering at the University of Queensland, Australia (email: rakic@itee.uq.edu.au)

I. Introduction

Vertical-Cavity, Surface-Emitting Lasers (VCSELs) have grown greatly in popularity and capability. Unlike conventional edge-emitting devices, VCSELs are designed with a very short resonant cavity, which suppourts a single longitudinal mode; light is emitted perpendicularly to the plane of crystal growth, allowing the construction of two-dimensional transmitter arrays for high bandwidth-density applications [1]–[6]. VCSELs have low threshold currents, high efficiencies, and can be tested on the wafer - minimising manufacturing costs [7].

VCSELs are heavily employed in high-bandwidth communications applications, and are particularly attractive candidates for use in optical interconnects. The maximum rate of direct modulation is limited by the interplay between photons and electrons, whose response can be characterised by a relaxation frequency, f_{r}, and damping frequency, Γ_{d}.

A general rule of thumb is that a directly modulated laser can suppourt a bit rate of up to 1.2 times its relaxation resonant frequency [8], however, the parasitics of device packaging and bonding can severely inhibit high frequency VCSEL performance [9], [10]. VCSEL chip bonding introduces capacitance from the pads and resistance from the leads; it is typically modelled as a first order RC circuit [11], [12]. The parasitics associated with packaged devices are more severe and tend to be represented by more complex circuit models [13], [14], but they still act as low pass filters. Any attempt to measure the intrinsic response of a VCSEL will have to account for the parasitic effects of the packaging and bonding, and also the associated frequency response of measurement equipment and driving circuitry. This can be achieved through accurate circuit modelling of the parasitics, intelligent signal processing to remove the effects numerically, or the observation of phenomena related to the intrinsic device properties, which will be immune to the parasitic effects.

In the work that follows, the high speed characteristics of a VCSEL are examined and related intrinsic parameters are extracted. Three different experimental techniques are employed to measure these quantities, and to compare the consistency of results between measurements, immunity to parasitics, ease of measurement, and miscellaneous factors, such as the availability of equipment and speed of measurement.

The nature of a VCSEL's small signal modulation response is investigated in section II; experimental processes are detailed in section III. The results for each approach are presented and compared in section IV, and a discussion relating to the difficulties and capabilities of each measurement technique follows in section V. Finally, conclusions are presented in section VI.

II. Small Signal Modulation Response

The intrinsic transient behaviour of VCSELs can be described by the rate equations, Eqs. (1)-(3) [15].

$$\frac{dS(t)}{dt} = \Gamma g \frac{N(t) - N_0}{1 + \epsilon S(t)} S(t) - \frac{S(t)}{\tau_{\mathrm{p}}} + \frac{\Gamma \beta N(t)}{\tau_{\mathrm{n}}} \tag{1}$$

$$\frac{dN(t)}{dt} = \frac{I(t)}{qV_{\mathrm{a}}} - g \frac{N(t) - N_0}{1 + \epsilon S(t)} S(t) - \frac{N(t)}{\tau_{\mathrm{n}}} \tag{2}$$

$$\frac{d\phi(t)}{dt} = \frac{\alpha\Gamma g}{2}(N(t) - N_{th}) \tag{3}$$

where,

N(t) is the carrier density,

S(t) is the photon density,

$\phi(t)$ is the optical phase,

I(t) is the drive current,

q is the electron charge,

V_{a} is the volume of the active region,

τ_{n} is the electron lifetime,

g is the gain slope constant,

α is the linewidth enhancement factor,

N_0 is the carrier density at transparency,

N_{th} is the carrier density at threshold,

ϵ is the nonlinear gain coefficient,

Γ is the optical confinement factor,

τ_{p} is the photon lifetime,

h is Planck's constant,

and β is the percentage of spontaneous emission that contributes to the lasing mode.

Photon density is analogous to optical power, $P(t)$, Eq. (4);

$$P(t) = \frac{V_{\mathrm{a}}\eta h\nu}{2\Gamma\tau_{\mathrm{p}}}S(t) \tag{4}$$

The phenomena described by these equations produce a second order frequency response [8], [9], [15]:

$$\frac{P(f)}{P_0} = \frac{f_{\mathrm{r}}^2}{f_{\mathrm{r}}^2 - f^2 + j\Gamma_{\mathrm{d}}\frac{f}{2\pi}} \tag{5}$$

$$\Gamma_{\mathrm{d}} = \frac{1}{2\tau_{\mathrm{n}}} + Kf_{\mathrm{r}}^2 \tag{6}$$

$$K = 2\pi^2(\tau_{\mathrm{p}} + \tau_{\mathrm{c}}) \tag{7}$$

$$f_{\mathrm{r}} = D\sqrt{P} = \sqrt{\frac{2\Gamma g\lambda}{V_{\mathrm{a}}hc}P} \tag{8}$$

where, ν is the lasing frequency; η is the quantum efficiency of the laser; τ_{p} is the photon lifetime; τ_{n} is the carrier lifetime; f_{r} is the relaxation resonant frequency; Γ_{d} is the damping frequency; P_0 is the optical power emitted with a 0 Hz driving signal; c and λ are respectively the speed and wavelength of the emitted light in free space. τ_{c}, D, and K are lumped parameters describing the relationship between the relaxation resonant and damping frequencies with optical power, P. These relationships indicate that a laser's high frequency response improves at high drive currents, and that the resonant peak will flatten with increasing drive current.

III. Experimental Procedures

The high-speed characterisation of VCSELs requires great care in the experimental design stages, the precise implementation of, often complicated, procedures, and very accurate, well calibrated high speed instrumentation. As a result, frequency related measurements are very difficult to perform and often inconsistent [16]. A number of techniques exist to measure the intrinsic, high-frequency VCSEL characteristics and extract the related parameters. These include

1) the measurement of the Relative Intensity Noise (RIN) [17],
2) fitting the S21 response to Eq. (5), and eliminating the response of other network elements [15],
3) examination of the optical spectrum at extremely high resolution to identify RF spectral artifacts [18]–[21], and
4) the observation of intermodulation and harmonic distortion effects [22], [23].

The first three of these techniques are performed on an *Avalon 850SM LA* VCSEL which emits strongly in the fundamental mode.

A. Relative Intensity Noise

Even with a noise free current source, variations will be present in a VCSEL's steady-state output, caused by spontaneous emission; these stochastic variations are referred to as Relative Intensity Noise (RIN) [24]. The quantity of noise can be calculated by considering the relative amounts of DC (laser power) optical power to AC (noise power) [25]:

$$RIN = \frac{\langle \delta P^2 \rangle}{\langle P \rangle^2} \tag{9}$$

In addition to determining the noise performance of a laser, the RIN measurement can also be used to examine its high frequency properties - a peak in noise power is present at the relaxation resonant frequency [26]. This phenomena relates to the intrinsic VCSEL properties, and is unaffected by the packaging and bonding parasitics. Both the average noise power, and severity of the resonant noise peak decrease with increasing drive current. The RIN can be fitted to Eq. (10) to extract the resonant and damping frequencies [27], [28].

$$RIN = \frac{A + B(2\pi f)^2}{16\pi^4 \left(f^2 - f_{\mathrm{r}}^2\right)^2 + (2\pi f)^2 \Gamma_{\mathrm{d}}^2} \tag{10}$$

Figure 2 shows the experimental setup employed to measure the relative intensity noise. The VCSEL is driven by a stable, constant current (*Newport 8000* modular controller), and the light is coupled into a *Newport D-100-FC* high-speed photodetector. The average optical power can be measured directly, and the RF component is transmitted through a DC block and two low-noise amplifiers (*Miteq JS2-00100800-17-0A* and *AFS3-00100800-32-L-N*). The noise characteristic is recorded by a microwave spectrum analyser (*Hewlett Packard 8565E*); the response of the detector, amplifiers, and the spectrum analyser's noise floor are numerically removed from these data to obtain the noise component of the VCSEL's output.

B. VNA Measurement

The small signal frequency response (S21) of the VCSEL (and associated circuitry) was measured with the *Rhode and Schwartz ZVCE* vector network analyser (VNA). A constant drive current was supplied to the VCSEL and a low power modulating signal was generated by the VNA. The VCSEL's RF output was measured by a high speed photodetector and compared to the original modulating source. The relationship between the two can be fitted to Eq. (5) to determine the relaxation resonant frequency and damping frequency of the VCSEL. The ideal S21 transmission curves are shown for a theoretical laser in Fig. 3.

A bias tee is used to combine the RF and DC current sources; a $50\ \Omega$ microstrip provides matched, low loss signal transmission; temperature is controlled by a peltier, which is thermally isolated from all other components.

While the values extracted from the RIN measurement and high resolution optical spectrum relate to the intrinsic VCSEL response, the S21 measurements implicitly contain package and bonding responses. These parasitics can be removed numerically, using the subtraction method suggested by [29]. The S21 of the VCSEL (and associated parasitics) at a reference drive current is subtracted from the response at other currents. It is assumed that the passive, parasitic elements are independent of current and the VCSEL response can be isolated. The resultant magnitude response should be of the form:

$$\mathrm{Mag}(f) = \frac{f_{\mathrm{r_I}}^4}{\left(f^2 - f_{\mathrm{r_I}}^2\right) + \left(\Gamma_{\mathrm{d_I}}/2\pi\right)^2 f^2} \times \frac{\left(f^2 - f_{\mathrm{r_0}}^2\right) + \left(\Gamma_{\mathrm{d_0}}/2\pi\right)^2 f^2}{f_{\mathrm{r_0}}^4} \tag{11}$$

where, $f_{\mathrm{r_0}}$ and $\Gamma_{\mathrm{d_0}}$ refer to the reference current and $f_{\mathrm{r_I}}$ and $\Gamma_{\mathrm{d_I}}$ refer to the response at current I.

Previous characterisation of the transmission line and bias tee indicate they are independent of current, and the detector exhibits no efficiency variations over the range of measurement. Under the reasonable assumption that package parasitics are also current independent, this technique greatly simplifies the circuit modelling requirements. Additionally, the calibration requirements are relaxed; instead of deconstructing and resoldering the laser jig between calibration and measurement, calibration can be performed before the bias tee and after the detector. A final experimental setup is shown below, Fig. 4.

C. High Resolution Optical Spectra

The phase noise of a laser is not spectrally flat, but instead has a resonance at the relaxation oscillation frequency [30], [31], similar to the peak observed in the RIN spectrum. This resonance manifests itself as a pair of spectral side bands, adjacent to each lasing mode in the optical spectrum. Like the RIN measurement, the spacing of these sidebands is unaffected by package parasitics, and can be used to determine the intrinsic relaxation resonant frequency of a laser. However, the relaxation resonant frequency is so small in comparison to the optical lasing frequency that these side peaks are not resolvable by conventional optical spectrum analysers - a 5 GHz spacing at 850 nm is approximately 0.01 nm.

An extremely high finesse optical cavity (*Newport SR-240-CF Supercavity*) was employed to identify these side bands. The supercavity is made up of two identical spherical lenses, which are controlled by piezo actuators. These mirrors form a non-confocal cavity - the spacing between the mirrors is greater than their radii of curvature - and the length of the cavity is varied periodically, changing the suppourted cavity resonant frequencies. In this way a high finesse ($> 10,000$) and high resolution (< 0.5 GHz) tunable, bandpass filter is implemented.

The experimental setup is shown in Fig. 5. Light which passes through the resonator is measured by a silicon photodetector. This weak signal is amplified by a low noise voltage amplifier, and observed on an oscilloscope. The piezo actuators are driven by a 30 Hz sawtooth wave. The output signal's variation with time can be converted to a relative frequency measurement, and from these data, the VCSEL's relaxation resonant frequency can be identified.

IV. Results

A. Relative Intensity Noise

The RIN profiles and fitted curves are shown for drive currents of 3.1 mA and 4.3 mA respectively, Figs. 6 and 7. The resonant peak can be observed in both figures, but an additional periodicity at higher drive currents indicates the formation of an external cavity. The frequency separation of these peaks confirm the cavity exists between points *A* and *B* (as marked in Fig. 2). The cavity can be disrupted by inserting a tilted neutral density filter in the path of the beam. Unfortunately, while a 10 dB optical attenuator removes the cavity effect, it also exacts a significant toll on the quality of the noise signal - the attenuated noise becomes almost unresolvable from the noise floor of the spectrum analyser.

An optical power meter was inserted into the experimental setup at point *C* to measure the level of optical feedback. A 3 dB beam splitter is used, so the measured reflections should be equal to the power coupled back into the VCSEL. The reflected signal was approximately -15 dB relative to the emitted laser power. While this level of feedback would significantly alter the performance of an edge emitting laser, VCSELs have shown much greater immunity to optical feedback as a result of their highly reflective mirrors. Bae *et al.* report VCSELs can be exposed to feedback levels as high as -13 dB without experiencing significant changes in operation [32]. In this case, the external cavity obscures the features of the noise signal and complicates extraction procedures, but shouldn't affect the parameters being measured.

In accordance with the theory, the resonant peak is sharpest at currents close to threshold, and the RIN decreases as optical power increases. Both the relaxation resonant frequency and damping frequencies were extracted at each current. Figures 13 and 14 show the progression of the relaxation resonant frequency and damping frequency with current; the results very closely resemble the expected proportionality between f_{r} and $\sqrt{I - I_{\mathrm{th}}}$. From the extracted parameters and Eq. (6), the carrier lifetime, τ_{n}, was found to be approximately 62.5 ps, and K was 0.3 ns.

B. VNA Measurement

The S21 response at 3.4 mA was chosen as the reference signal, and a multi-variable global parameter extraction was performed on the subtracted responses to obtain the relaxation resonant and damping frequencies of the VCSEL. An unfortunate side effect of the subtraction method relates to the resonances induced by the external cavity; the resonant peaks of this external cavity become slightly misaligned with each other as drive current is increased. While this doesn't affect VCSEL performance, it does amplify the effect of these resonances on parameter extraction - even small oscillations become problematic. A tilted optical attenuator can be used (in this case) to reduce reflections without sacrificing the sensitivity of the vector network analyser, however, additional resonances can still be observed in the subtracted S21 plots. As before, these reflections are of sufficient strength to complicate parameter extraction, but not strong enough to significantly alter VCSEL operation.

Figures 8 and 9 show the raw S21 response of the VCSEL at 2.8 mA and the resultant response after the reference characteristic has been subtracted. The extracted relaxation resonant and damping frequencies are compared to the results from the other measurements in Fig. 13 and 14; τ_{n} was calculated as 68.1 ps and K = 0.34 ns.

C. High Resolution Optical Spectra

The supercavity suppourts both longitudinal modes, with a spacing of 7853 GHz, and transverse modes, with a separation of 28.66 GHz. Each transverse VCSEL mode can couple with every supercavity mode, creating extremely complicated spectral structures. Furthermore, the slight frequency non-degeneracy between same order transverse modes, and the birefringence-induced frequency splitting between modes of different polarisations, may also be resolvable. The VCSEL transverse modes can be identified as a family of peaks as each mode couples with the fundamental, and transverse modes of the supercavity.

Before the relaxation resonant frequency can be measured, three obstacles must be overcome:

1) the features must be identified;
2) the time scale must be converted to frequency; and
3) the system must be calibrated.

The spectra of the VCSEL (operating in its single mode regime) is shown in Fig. 10. The majority of these features can be clearly identified. The strongest peak is the fundamental Gaussian mode coupled with the fundamental cavity mode; on both sides of this mode, equally spaced sidebands, corresponding to the relaxation resonant frequency, can be observed. The second largest feature is the fundamental VCSEL mode coupled with a transverse cavity mode; a resonant sideband can also be identified, accompanying this mode. The final feature is not so readily identifiable

- the spacing is too small for it to be another transverse cavity mode, and far too small to be a transverse VCSEL mode. The most likely explanation is that it represents the fundamental mode, lasing in another polarisation.

The resonant, longitudinal modes of a cavity are determined by the familiar relationship [33]:

$$L = \frac{mc}{2nf_m} \tag{12}$$

where, L is the length of the cavity, n is the refractive index, and m is an integer representing the mode number. If a variable length cavity with mirrors moving at speed u is considered,

$$f_m(t) = \frac{mc}{2n(L+ut)} \tag{13}$$

The mirrors of the supercavity move at a constant rate, meaning the relative frequency of features will not be proportional with time, and the scales can not be simply converted to frequency. The known frequency spacing between transverse cavity modes (28.66 GHz) can be used to calibrate the results. Figure 11 shows the unequal spacing between consecutive supercavity transverse modes. From this plot, the relationship between time and frequency can be determined, Fig. 12; all values are relative to the fundamental mode.

Unfortunately, the calibration performed at one current is not strictly valid for other drive currents. As the current increases, the lasing wavelength drifts and the supercavity sweep parameters have to be changed to ensure the entire spectrum is viewable. However, the frequency-time relationship is well behaved, and over small frequency ranges, a linear conversion seems reasonable. The high resolution, optical spectra for a range of currents were recorded, and are shown in Fig. 13; the data were calibrated with respect to the first transverse cavity mode.

Over the current range shown, the side bands corresponding to the VCSEL's relaxation resonant frequency could be clearly identified. At lower drive currents, the emitted beam couldn't be coupled strongly enough into the cavity to resolve the bands; at higher currents, the side bands are too heavily damped to identify. Typically, the relaxation resonant frequency is considered to be linear with $\sqrt{I - I_{\mathrm{th}}}$, but this relationship is only accurate at low photon densities or when heating effects are negligible [16]. The measurement range covered in these experiments extends into the region of VCSEL operation where the fundamental mode has started to decay. In this case, the relaxation resonant frequency should be considered with respect to the square root of optical power.

D. Comparison of Results

The relaxation resonant frequency is plotted against the square root of optical power of the fundamental mode, Fig. 13. The relaxation resonant frequency increases linearly with $\sqrt{P}$ in excellent agreement with the expected trend [27]:

$$f_r = D\sqrt{P} \tag{14}$$

The parameter D was calculated as 6.93, 7.25, and 5.67 GHz/$\sqrt{\mathrm{mW}}$ for the RIN, VNA, and supercavity measurements respectively. While the RIN and VNA measurements show outstanding correlation, the relaxation

resonant frequencies measured by the supercavity are consistently slightly lower. The most likely explanation for this discrepancy is calibration.

The damping frequencies, Γ_d, can also be extracted from the RIN and VNA measurements, Fig. 14, and they show the same excellent agreement.

V. Discussion

Experiments have been performed to measure the relaxation resonant and damping frequencies using three different techniques: identification of the RIN peak, extraction from the S21 profile (as measured by the vector network analyser), and observation of the resonant side bands in the optical spectrum. Results for all three techniques were consistent and in line with theory and previously noted experimental trends. A summary of the characteristics and capabilities of each procedure is given in Tab. I, and further discussion follows below.

While all three methods were employed to extract the same parameters, there is a stark difference in application and measurement philosophy between the three techniques.

The RIN measurement was powerful - both f_r and Γ_d could be extracted - and simple - the noise could be measured using the same laser driver and thermal control as DC measurements, and only a high-speed photodetector, low-noise amplifiers, and an RF spectrum analyser were required. Furthermore, the RIN characteristic is isolated from package and bonding parasitics; the noise measurement represents the intrinsic properties of the laser under test.

Despite the mild appearance of Eq. (10), fitting and parameter extraction proved very difficult in practice. The thermal noise of the amplifiers and photodetector, as well as the detector's shot noise, conspire to raise the noise floor of the RFSA, decreasing the dynamic range of the RIN measurement. The relaxation resonant frequency can still be extracted easily, but the accuracy of the extracted damping frequency depends strongly on the initial estimate. The extraction of frequency related parameters from the RIN becomes more difficult as drive current increases. The high-speed response of the photodetector limits the RIN measurements as current and relaxation resonant frequency increase, but more importantly higher order modes complicate the noise characteristic. Multiple peaks in the RIN signal have been observed when the contribution of higher order modes becomes significant; the secondary peaks have been variously explained as the relaxation resonant frequencies of the transverse modes [34], [35] or as the mode partition noise [28]. Regardless of the cause, the added complexity greatly complicates an already difficult parameter extraction procedure.

The measurement and analysis of a laser's S21 share the difficulties and characteristics of electrical network analyser measurements: results depend heavily on the quality of calibration. As demonstrated by the subtraction technique, the burdens of calibration can be reduced through superior signal processing; conversely, thorough calibration and circuit design procedures make parameter extraction easier. However, neither experiment nor analysis can be performed rigorously enough to completely eliminate reliance on the other. If both aspects are addressed, the network analyser can be used to accurately determine the relaxation resonant and damping frequencies, as well

as the reflection characteristics of the device and packaging. However, like the RIN measurement, the presence of higher-order lasing modes increases the difficulty of performing accurate parameter extractions.

Alone amongst the experiments conducted, the S21 measurement requires high-speed operation of the VCSEL, which necessitates the design of suitable driving circuitry and careful consideration of calibration points. Once the initial design issues have been overcome, the S21 is an extremely simple measurement to make. This technique benefits greatly from the legacy of microwave measurements and accumulated knowledge, and unlike high-finesse optical cavities, network analysers are ubiquitous in laboratory environments.

Despite the power and availability of network analysers, the S21 is an inherently non-ideal measurement for this particular application (extraction of intrinsic laser parameters). The VCSEL's transfer function is complicated by package and bonding parasitics, which are non-trivial to remove. The use of a probing station on VCSEL chips reduces the problems caused by parasitics, but doesn't eliminate them completely. If possible, it is far more appealing to measure the intrinsic parameters directly. The network analyser measurements seem more suitable for use in higher level analysis, such as integrated transmitter characterisation, in which the parasitic response is as important as the VCSEL characteristics.

Analysis of the optical spectrum is neither as popular nor powerful as the previous two measurement techniques. The side bands are spaced too closely to resolve with conventional instruments, and only the relaxation resonant frequency can be determined from these bands. The relative strength of the peaks decreases with drive current, suggesting the damping frequency could also be calculated. However, their magnitude is affected by the gain spectrum of the VCSEL, and their existence is not yet understood well enough to accurately model their behaviour.

In measuring the relaxation resonant frequency alone, spectral analysis is a very attractive procedure. The phase noise is isolated from package parasitics; the bulk of the experimental setup is shared with DC characterisation procedures; optical power is measured at DC, so the operational range is not limited by the speed of the photodetector; and the relaxation resonant frequency can be determined almost immediately from the initial data - time consuming parameter extractions are avoided. Unfortunately, the supercavity employed is neither user friendly, flexible, nor robust; calibration is a problem area; and the optical sidebands are weak and difficult to identify. The implementation of a heterodyning spectrum analyser, instead of a supercavtiy, could reduce these problems, but will not eliminate them.

For all its difficulties, this technique seems very promising - it addresses the shortcomings of other measurements. In amplitude based measurements, such as the RIN and S21, the contributions of transverse modes are superimposed and unresolvable; in spectral measurements, the modes remain spectrally separated and can easily be distinguished from each other. The lasing of higher order modes will not hinder the measurement of the fundamental mode's relaxation resonant frequency. In fact, if sufficient power could be coupled from the transverse modes, the relaxation resonant frequency of each mode could be measured simultaneously.

VI. Conclusions

The S21 measurement is, in essence, *electrical*, and it inherits the familiar difficulties and requirements: well matched driving circuitry, low attenuation at all frequencies, and rigorous calibration conducted as close to the device as possible. By contrast, the supercavity provides an *optical* measurement; success relies heavily on alignment, mode matching, coupling power, and the quality of optical components. The RIN measurement falls somewhere in between - it measures a fundamental optical characteristic (spontaneous emission), but in the electrical domain. Through this fortunate combination, it is burdened little by either electrical or optical concerns.

In the final analysis, the supercavity measurement seems the most promising and underdeveloped; the VNA measurement, the most convenient and familiar; and the RIN measurement, the most robust. The three techniques provide consistent results, but possess clear advantages for various situations.

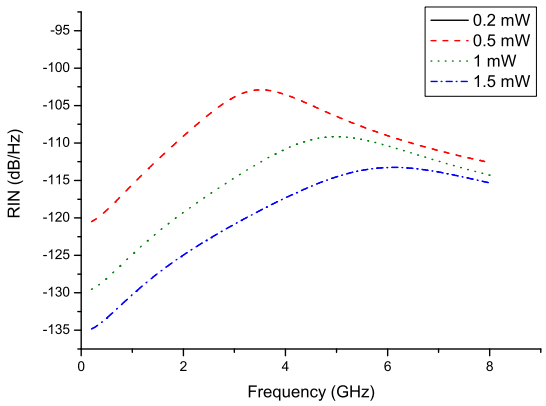

Fig. 1: Theoretical RIN, according to Eq. (10), for increasing power. The resonant and damping frequencies are $\{3.53,\ 11.2\}$, $\{5,\ 20.5\}$, and $\{6.12,\ 26.75\}$ GHz for VCSEL powers of $0.\ 5$mW, 1 mW, and 1.5 mW respectively.

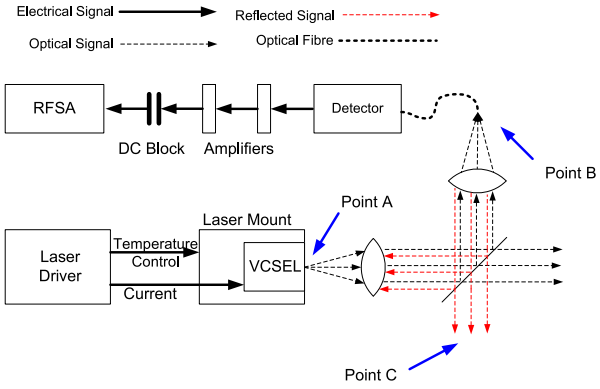

Fig. 2: Experimental setup used to measure the relative intensity noise.

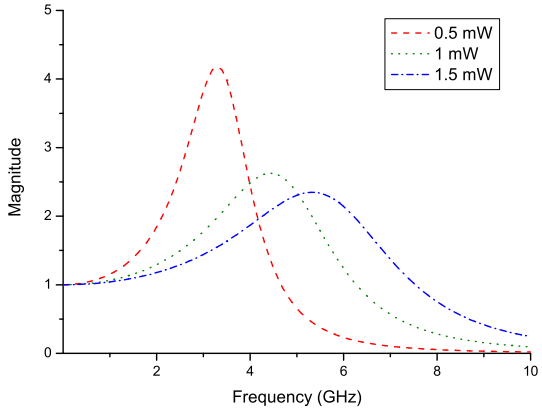

Fig. 3: Theoretical S21 for increasing power. The resonant and damping frequencies are $\{3.53, 11.2\}$, $\{5, 20.5\}$, and $\{6.12, 26.75\}$ GHz for VCSEL powers of 0.5mW, 1 mW, and 1.5 mW respectively.

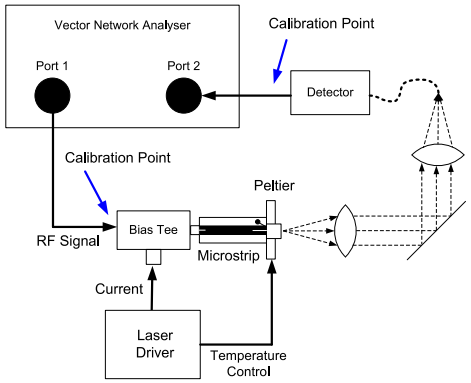

Fig. 4: Experimental setup used to measure VCSEL frequency response.

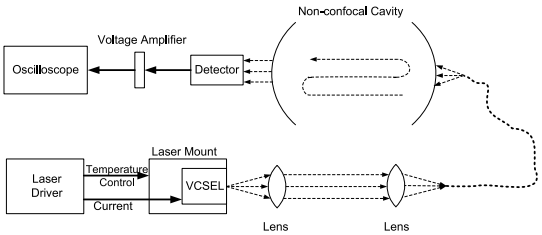

Fig. 5: Experimental setup used to obtain high-resolution, optical VCSEL spectra.

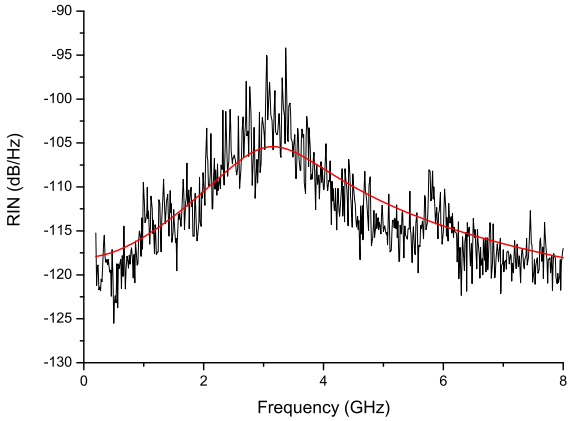

Fig. 6: Relative Intensity Noise for the VCSEL at a 3.1mA drive current. A resonant peak can be observed at 3.2GHz.

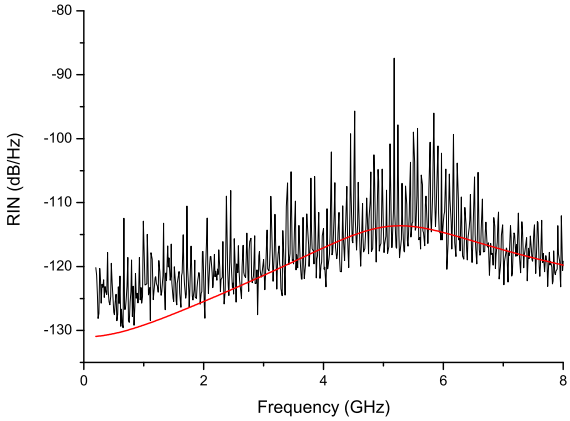

Fig. 7: Relative Intensity Noise for the VCSEL at a 4.3mA drive current. A resonant peak can be observed at 5.3GHz.

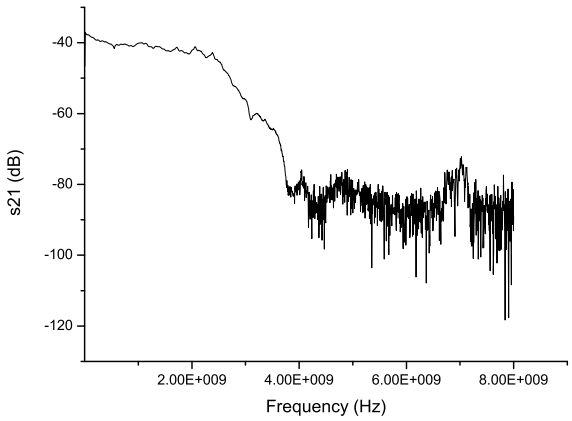

Fig. 8: S21 response at 2.8 mA drive current.

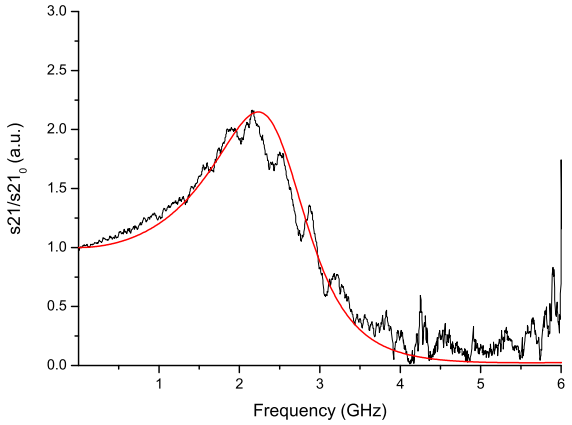

Fig. 9: Subtracted S21 response of the VCSEL at 2.8 mA drive current.

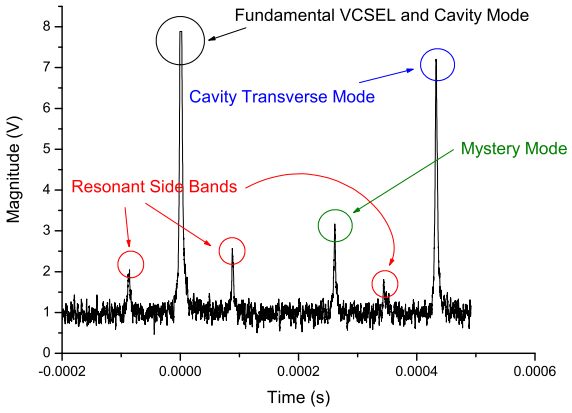

Fig. 10: Spectral structure of the VCSEL at 6 mA after it has been passed through the supercavity

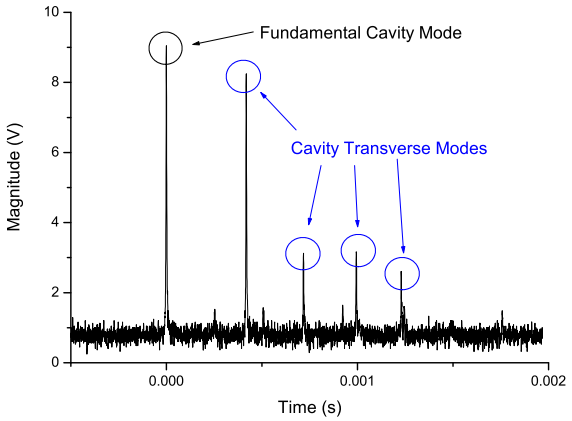

Fig. 11: Long time scale, spectral structure of the VCSEL at 5.5 mA after it has been passed through the supercavity

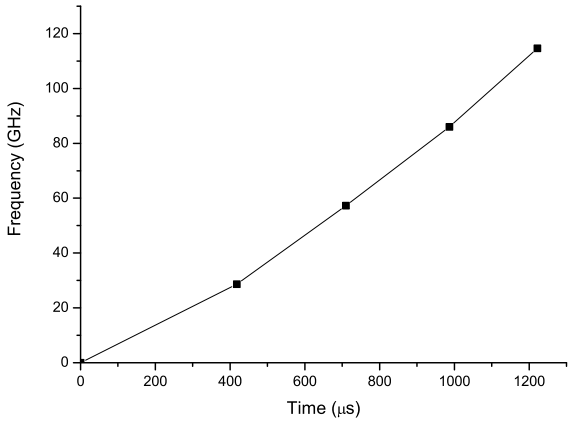

Fig. 12: Relationship between relative frequency and time, used to calibrate the supercavity

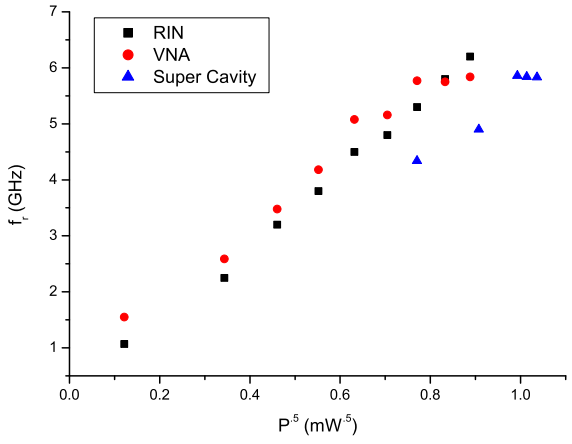

Fig. 13: Measured relaxation resonant frequencies of the VCSEL.

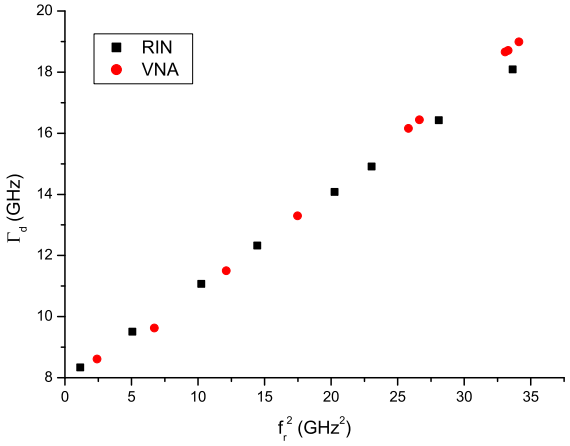

Fig. 14: Measured damping frequencies of the VCSEL.

TABLE I: Comparison of measurement techniques.

	VNA	RIN	Optical Spectra
Immunity to parasitics	Poor	Excellent	Excellent
Immunity to optical feedback	Low	Low	High
Ease of measurement	Average	Very Easy	Difficult
Parameter extraction	Difficult	Difficult	Very Easy
Availability of instruments	Very High	Very High	Low
Damping Frequency?	Yes	Yes	Qualitative

REFERENCES

[1] M. Forbes, J. Gourlay, and M. Desmulliez, "Optically interconnected electronic chips: A tutorial and review of the technology," *Electronics and Communication Engineering Journal*, vol. 13, pp. 221–231, October 2001.

[2] S. Tang, R. T. Chen, L. Garrett, D. Gerold, and M. M. Li, "Design limitations of highly parallel free-space optical interconnects based on arrays of vertical cavity surface-emitting laser diodes, microlenses and photodetectors," *J. Lightwave Technol.*, vol. 12, pp. 1971–1975, November 1994.

[3] N. McArdle, M. Naruse, and M. Ishikawa, "Optoelectronic parallel computing using optically interconnected pipelined processing arrays," *IEEE Select. Topics Quantum Electron.*, vol. 5, pp. 250–260, March/April 1999.

[4] Y. Liu, "Heterogeneous integration of OE arrays with si electronics and microoptics," *IEEE TRANS ADV PACK*, vol. 25, pp. 43–49, February 2002.

[5] L. A. Coldren, O. Sjolund, D. A. Louderback, S. Nakagawa, and E. R. Hegblom, "Flip-chip bonded, back emitting, microlensed arrays of monolthic vertical cavity lasers and resonant photodetectors," *Electronic Components and Technology Conference*, pp. 733–740, 1999.

[6] A. Karim, J. Piprek, P. Abraham, D. Lofgreen, Y. Chiu, and J. E. Bowers, "1.55-um vertical-cavity laser arrays for wavelength-division mulitplexing," *IEEE J. Quantum Electron.*, vol. 7, pp. 178–183, March/April 2001.

[7] L. A. Coldren, *Diode Lasers and Photonic Integrated Circuits*. John Wiley, New York, 1995.

[8] J. E. Bowers, "High speed semiconductor laser design and performance," *Solid-St. Electron.*, vol. 30, no. 1, pp. 1–11, 1987.

[9] K. Petermann, *Laser Diode Modulation and Noise*. Kluwer Academic Publishers, 1991.

[10] S. Z. Zang, N. M. Margalit, T. E. Reynolds, and J. E. Bowers, "1.54 μm vertical-cavity surface-emitting laser transmission at 2.5 GB/s," *IEEE Photon. Technol. Lett.*, vol. 9, pp. 374–376, 1997.

[11] K. Czotscher, S. Weisser, A. Levin, and J. Rosenzweig, "Intensity modulation and chirp of 1.55-um multiple-quantum-well laser diodes: Modeling and experimental verification," *IEEE Select. Topics Quantum Electron.*, vol. 5, pp. 606–612, May/June 1999.

[12] K. A. Black, E. S. Bjorlin, J. Piprek, E. Hu, and J. E. Bowers, "Small-signal frequency response of long-wavelength vertical-cavity lasers," *IEEE Photon. Technol. Lett.*, vol. 13, pp. 1049–1051, October 2001.

[13] M. Bruensteiner and G. C. Papen, "Extraction of VCSEL rate-equation parameters for low bias system simulation," *IEEE Select. Topics Quantum Electron.*, vol. 5, pp. 487–494, May/June 1999.

[14] J. K. Guenter, J. A. Tatum, A. Clark, R. S. Penner, R. H. Johnson, R. A. Hawthorne, J. R. Biard, and Y. Liu, "Commercialization of honeywell's VCSEL technology: Further developments," *Proc. of the SPIE*, vol. 4286, 2001.

[15] L. Bjerkan, A. Royset, L. Hafskjaer, and D. Myhre, "Measurement of laser parameters for simulation of high-speed fiberoptic systems," *J. Lightwave Technol.*, vol. 14, pp. 839–850, May 1996.

[16] G. Guekos, *Photonic Devices for Telecommunications: How to Model and Measure*. Berlin: Springer, 1999.

[17] D. Tauber, G. Wang, R. S. Geels, J. E. Bowers, and L. A. Coldren, "Large and small signal dynamics of vertical cavity surface emitting lasers," *Appl. Phys. Lett.*, vol. 62, pp. 325–327, January 1993.

[18] S. Jiang, M. Dagenais, and R. A. Morgan, "Optical spectrum sidebands of a vertical-cavity surface-emitting laser," *Proc. IEEE/LEOS Annual Meet.*, vol. 1, pp. 278–279, 1994.

[19] K. Vahala, C. Harder, and A. Yariv, "Observation of relaxation resonance effects in the field spectrum of semiconductor lasers," *Appl. Phys. Lett.*, vol. 43, pp. 211–213, 1983.

[20] C. H. Henry, "Theory of the phase noise and power spectrum of a single mode injection laser," *IEEE J. Quantum Electron.*, vol. 19, pp. 1391–1397, 1983.

[21] C. H. Henry, "Phase noise in semiconductor lasers," *J. Lightwave Technol.*, vol. 4, pp. 298–311, 1986.

[22] T. E. Darcie, R. S. Tucker, and G. J. Sullivan, "Intermodulation and harmonic distortion in InGaAsP lasers," *Electron. Lett.*, vol. 21, pp. 665–666, 1985.

[23] M. Majewski and L. Coldren, "Distortion characteristics in directly modulated laser diodes by microwave signals," *IEEE 1989 MTT-S International Microwave Symposium Digest (Cat. No.89CH2725-0)*, pp. 1167 – 70, 1989//. DFB lasers;semiconductor lasers;harmonic distortion;spectra measurements;directly modulated laser diodes;intermodulation distortion characteristics;microwave analog signals;small-signal perturbation analysis;rate equations;damping factor;resonant frequency;small-signal modulation response;de-embedding procedure;distributed feedback;1.3 micron;1.5 micron;6 GHz;.

[24] K. Petermann, “External optical feedback phenomena in semiconductor lasers,” *IEEE Select. Topics Quantum Electron.*, vol. 1, pp. 480–489, June 1995.

[25] G. E. Obarski and P. D. Hale, “How to measure relative intensity noise in lasers,” *Laser Focus World*, pp. 273–277, 1999.

[26] D. M. Kuchta, J. Gamelin, J. D. Walker, J. Lin, K. Y. Lau, J. S. Smith, M. Hong, and J. P. Mannaerts, “Relative intensity noise of vertical cavity surface emitting lasers,” *Appl. Phys. Lett.*, vol. 62, pp. 1194–1196, March 1993.

[27] M. C. Tatham, I. F. Lealman, C. P. Seltzer, L. D. Westbrook, and D. M. Cooper, “Resonance frequency, damping, and differential gain in $1.5\mu m$ multiple quantum-well lasers,” *IEEE J. Quantum Electron.*, vol. 28, pp. 408–414, 1992.

[28] L.-G. Zei, S. Ebers, J.-R. Kropp, and K. Petermann, “Noise performance of multimode VCSELs,” *J. Lightwave Technol.*, vol. 19, pp. 884–892, June 2001.

[29] P. A. Morton, T. Tanbun-Ek, R. A. Logan, A. M. Sergent, P. F. Sciortino, and D. L. Coblentz, “Frequency response subtraction for simple measurement of intrinsic laser dynamic properties,” *IEEE Photon. Technol. Lett.*, vol. 4, pp. 133–136, 1992.

[30] S. Piazzolla, P. Spano, and M. Tamburrini, “Characterization of phase noise in semiconductor lasers,” *Appl. Phys. Lett.*, vol. 41, pp. 696–696, 1982.

[31] B. Daino, P. Spano, M. Tamburrini, and S. Piazzolla, “Phase noise and spectral line shape in semiconductor lasers,” *IEEE J. Quantum Electron.*, vol. 19, pp. 266–270, 1983.

[32] J. W. Bae, H. Temkin, S. E. Swirhun, W. E. Quinn, P. Brusenbach, C. Parsons, M. Kim, and T. Uchida, “Reflection noise in vertical cavity surface emitting lasers,” *Appl. Phys. Lett.*, vol. 63, pp. 1480–1482, 1993.

[33] J. T. Verdeyen, *Laser Electronics*. Prentice Hall, New Jersey, 1995.

[34] Y. Satuby and M. Orenstein, “Small-signal modulation of multitransverse modes vertical-cavity surface-emitting semiconductor lasers,” *IEEE Photon. Technol. Lett.*, vol. 10, pp. 757–759, June 1998.

[35] A. Valle and L. Pesquera, “Relative intensity noise of multitransverse mode vertical cavity surface emitting lasers,” *Proc. CLEO’99*, 1999.

Christopher J. O’Brien was born in Adelaide, Australia in 1980. He received a bachelor of electrical engineering from the University of Queensland in 2001, and is currently a Ph.D candidate at the same institution. Primary research interests are the experimental investigation and modelling of vertical-cavity, surface-emitting lasers - particularly in a free-space optical interconnect environment.